VIP Imaging Agents Very Important Paper

DOI: 10.1002/ange.201304465

# PEGylation and Zwitterionization: Pros and Cons in the Renal Clearance and Tumor Targeting of Near-IR-Emitting Gold Nanoparticles**

*Jinbin Liu, Mengxiao Yu, Xuhui Ning, Chen Zhou, Shengyang Yang, and Jie Zheng**

PEGylation is the most common and successful surface modification for reducing nonspecific accumulation and prolonging the blood circulation of inorganic nanoparticles (NPs) so that they can effectively target tumors through the well-known enhanced permeability and retention (EPR) effect.[1] These strengths fundamentally arise from the fact that poly(ethylene glycol) (PEG) moieties on the particle surface create steric hindrance for serum protein (opsonin) adsorption and slow down NP uptake by the reticuloendothelial system (RES) organs, such as the liver and spleen.[2] However, the majority of PEGylated NPs still end up in the RES organs after circulation,[3] thus resulting in low targeting specificity (defined as the amount of NPs in the tumor versus that in the liver).[4] For instance, even though PEGylated AuNPs with a 2 nm core size can circulate in the body at a high concentration, they were found to significantly accumulate in the liver (78 % ID $g^{-1}$; ID = injected dose) and spleen (15.2 % ID $g^{-1}$) at 24 h post injection (p.i.).[5] Such long-term severe accumulation in the RES potentially induces health hazards, thus hampering the clinical translation of NPs. Therefore, developing PEGylated inorganic NPs that not only retain a strong EPR effect but can also be eliminated from the urinary system like clinically used small-molecule contrast agents[6] is highly desired but remains a big challenge.

The high RES uptake of PEGylated inorganic NPs essentially results from their large hydrodynamic diameters (HDs), which are above the kidney filtration threshold (ca. 5.5 nm).[7] For instance, for 2 nm AuNPs, the HDs increased to 9–10 nm after PEGylation.[5] To develop renal-clearable PEGylated quantum dots (QDs), Choi and co-workers investigated the influence of PEG length (PEG-$n$, $n = 2$, 3, 4, 8, 14, 22) on the renal clearance of QDs and observed efficient renal clearance of the QDs conjugated with PEG-4.[8] PEG ligands with other lengths failed to enhance the renal clearance of QDs as a result of either large HDs or low physiological stability.[8] However, the tumor targeting properties of the renal-clearable PEGylated QDs still need to be investigated. Silica NPs of approximately 7 nm coated with 0.5 kDa PEG were also renal-clearable,[9] but the passive tumor-targeting efficiency was only 0.9 % ID $g^{-1}$ at 4 h p.i.[10]

To avoid significant increases in HD, surface chemistry based on zwitterionic ligands was used in the development of renal-clearable NPs.[11] For example, the HDs of 3 nm QDs and 2.5 nm luminescent AuNPs were only 4.9 nm and 3.4 nm in the presence of serum protein after being coated with cysteine (CS-QDs)[11a] or glutathione (GS-AuNPs),[11h] respectively; as a result, they were effectively eliminated from the urinary system (CS-QDs: > 65 % ID, 4 h p.i.; GS-AuNPs: > 60 % ID, 48 h p.i.).[11a,g] However, the short retention times and low concentrations of these renal-clearable NPs in the blood compromised their effectiveness in passive tumor targeting through the EPR effect. Consequently, the tumor contrast was only enhanced approximately 80 % over normal mouse tissues after injection with the CS-QDs.[11b] Overall the tumor-targeting efficiency of the GS-AuNPs was only 2.3 % ID $g^{-1}$ at 12 h p.i.[11h]

The low tumor-targeting efficiencies of these known renal-clearable zwitterionic NPs raise a new challenge for the translation of inorganic NPs into clinical practice. In addition, fundamental understanding of how PEGylation and zwitterionization influence the renal clearance and tumor targeting of renal-clearable NPs is still missing. To address these challenges, we created renal-clearable PEGylated near-IR-emitting AuNPs (NIR-emitting PEG-AuNPs) with photophysical properties, core sizes, low affinity to serum protein, and high physiological stability almost identical to our reported zwitterionic NIR-emitting GS-AuNPs (Figure S1 in the Supporting Information).[11h] By conducting a head-to-head comparison of these two NPs with respect to renal clearance and tumor targeting, we were able to unravel the pros and cons of these two surface modifications in the tumor-imaging properties of luminescent AuNPs. Our results show that the NIR-emitting PEG-AuNPs exhibit efficient renal clearance and low RES accumulation compared to the NIR-emitting GS-AuNPs: more than 50 % ID were excreted in the urine and only less than 4 % ID $g^{-1}$ had accumulated in the liver 24 h p.i. However, these two types of renal-clearable luminescent AuNPs are significantly different with respect to tumor targeting. The fundamental understanding of the strengths and limitations of these two surface modifications in the tumor targeting of renal-clearable AuNPs provides a foundation for the design of a new generation of renal-clearable AuNPs for future clinical practice.

[*] Dr. J. Liu, Dr. M. Yu, X. Ning, Dr. C. Zhou, Dr. S. Yang, Prof. Dr. J. Zheng
Department of Chemistry
The University of Texas at Dallas
800 W. Campbell Rd. Richardson, Texas, 75080 (USA)
E-mail: jiezheng@utdallas.edu
Homepage: http://www.utdallas.edu/~jiezheng

[**] This work was supported in part by the NIH (R21EB009853 to J.Z.), CPRIT (RP120588) and the start-up fund from the University of Texas at Dallas (J.Z.). X.N. acknowledges the Office of Sponsored Research for an undergraduate research award.

Supporting information for this article is available on the WWW under http://dx.doi.org/10.1002/anie.201304465.

  

The NIR-emitting PEG-AuNPs were created through a facile one-step synthesis by thermally reducing $HAuCl_4$ in the presence of thiolated PEG (PEG-SH) ligands with a molecular weight (MW) of 1 kDa (ca. 21 units) in aqueous solution (Figure 1 a and Figure S2 in the Supporting Information). Neither shorter (0.35 kDa) nor longer (5 kDa) PEG ligands generated highly luminescent or stable AuNPs (Figures S3 and S4 in the Supporting Information). The core size of the PEG-AuNPs was measured to be $(2.3 \pm 0.3)$ nm, between the PEG-AuNPs and the GS-AuNPs make it feasible to conduct a head-to-head comparison of their renal clearance and tumor targeting under the same imaging conditions.

To quantify tumor-targeting efficiency and specificity, mice bearing MCF-7 tumors were used as a model system, and the biodistribution of the PEG-AuNPs in the mice at the selected p.i. time points (1, 12, 24, and 48 h) was measured by using inductively coupled plasma mass spectrometry (ICP-MS, Figure 2 a). The tumor-targeting efficiencies of the PEG-

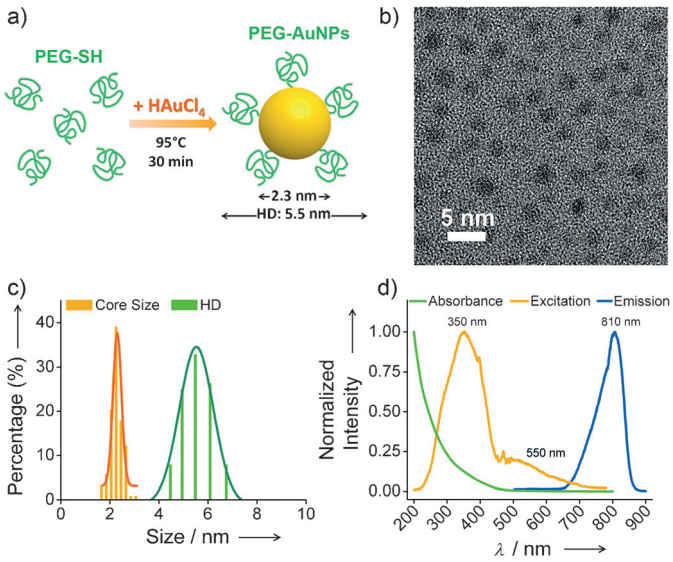


***Figure 1.*** Characterization of NIR-emitting PEGylated AuNPs (PEG-AuNPs). a) Scheme of the particle synthesis. b) Typical TEM image of the synthesized PEG-AuNPs. c) Core size measured by TEM, and hydrodynamic diameter (HD) in phosphate-buffered saline (PBS) measured by dynamic light scattering (DLS). d) Absorption, excitation, and emission ($\lambda_{exc} = 350$ nm) spectra of the PEG-AuNPs in PBS at pH 7.4.

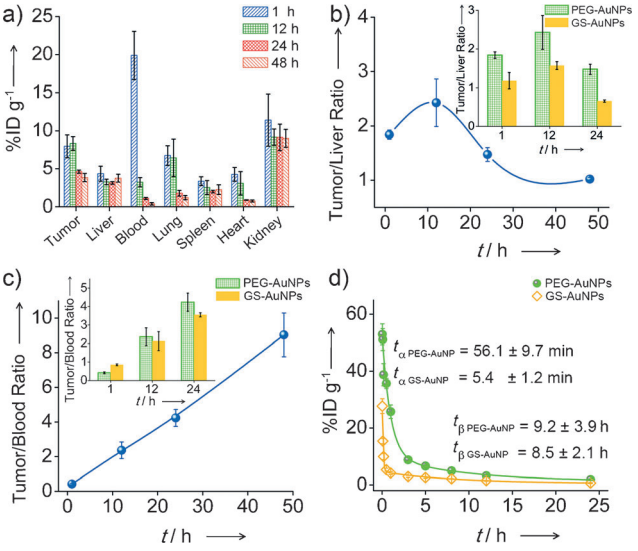


***Figure 2.*** Biodistribution analysis of passive tumor targeting in mice bearing MCF-7 tumors. a) Biodistributions of the PEG-AuNPs at 1, 12, 24, and 48 h p.i. b) The time-dependent ratios of PEG-AuNP concentration in the tumor relative to that in the liver (tumor/liver ratios) over the 48 h p.i. (Inset: a comparison of the tumor/liver ratios of the PEG-AuNPs and the GS-AuNPs at 1, 12, and 24 h p.i.). c) The time-dependent tumor/blood ratios of the PEG-AuNPs over the 48 h p.i. (Inset: a comparison of tumor/blood ratios of the two probes at 1, 12, and 24 h p.i.). d) Pharmacokinetics of the two probes after intravenous (iv) injection (data presented as the mean ± standard deviation, $n = 3$).

very similar to that of the GS-AuNPs (2.5 nm), but their HD ($(5.5 \pm 0.4)$ nm) was slightly larger than that of the GS-AuNPs (3.3 nm; Figure 1 b,c). Such a large increase in HD after PEGylation in comparison with zwitterionic ligand coating was in agreement with previous findings.[14] However, the HD layer of the PEG-AuNPs (1.6 nm) is much thinner than those of the reported PEGylated 2 nm AuNPs (3.5–4 nm),[5] and comparable to the calculated Flory radius (F, ca. 1.9 nm) of PEG (MW, 1 kDa) in "mushroom" conformation on the AuNP surface,[1c] thus suggesting a relatively low-density structure for PEG on the particle surface rather than a high-density extended structure.[14]

The PEG-AuNPs exhibited strong emission with a maximum at 810 nm and broad excitation with peaks at 350 and 550 nm (Figure 1 d), values identical to those for the GS-AuNPs,[11h] thus suggesting that these surface modifications have little influence on the luminescence of AuNPs. In addition, like the GS-AuNPs,[11h] the NIR-emitting PEGylated AuNPs also exhibit high physiological stability (Figure S5 in the Supporting Information) and high resistance to serum protein adsorption after being incubated in mouse serum protein at 37 °C for 48 h (Figure S6 in the Supporting Information). These similarities in photophysical properties

AuNPs were determined to be $(8.0 \pm 1.5)$ and $(8.3 \pm 0.9)$ % ID $g^{-1}$ at 1 and 12 h p.i., respectively. These values were approximately three and ten times higher than those for the GS-AuNPs (2.3 % ID $g^{-1}$ at 12 h p.i.)[11h] and renal-clearable silica NPs (0.9 % ID $g^{-1}$),[10] respectively. The targeting efficiency of approximately 8 % ID $g^{-1}$ was also comparable to those of reported NPs that have strong EPR effects but are not renal-clearable, such as PEGylated 20 nm AuNPs (6.63 % ID $g^{-1}$),[12b] and six-armed PEGylated $Ag_2S$ QDs (10 % ID $g^{-1}$).[12c] In terms of liver uptake of the PEG-AuNPs, the maximum accumulation was 4.35 % ID $g^{-1}$ at 1 h p.i. and the amount remained roughly constant (3.27–3.76 % ID $g^{-1}$) during the subsequent 48 h, a result comparable to the liver accumulation of the GS-AuNPs.[11g,h] Since the clearance of the PEG-AuNPs was different in tumor and liver, the targeting specificity was time-dependent (Figure 2 b) and reached its maximum of $2.4 \pm 0.4$ at 12 p.i., a value higher than that for the GS-AuNPs ($1.6 \pm 0.1$)[11h] and nearly two orders of magnitude better than any known AuNPs that are not renal

clearable.[1a,12b,13] The difference in tumor versus liver uptake behaviors between the PEG-AuNPs and the GS-AuNPs suggests that the PEGylation of renal-clearable AuNPs could further enhance tumor-targeting specificity without sacrificing their low RES uptake.

The origin of the high tumor-targeting efficiency of these NIR-emitting PEG-AuNPs can be attributed to their strong EPR effect enhanced by PEGylation. To determine how well the EPR effect functions, the tumor/blood ratio of the probes is typically measured.[1e] The tumor/blood ratio of the PEG-AuNPs steadily increased with time and reached $9.0 \pm 1.3$ at 48 h p.i., a result consistent with many known NPs that have strong EPR effects but are not renal-clearable (Figure 2c). For example, the tumor/blood ratio ($4.2 \pm 0.5$) of the PEG-AuNPs at 24 h p.i. was higher than those of both PEG-coated 33 nm gold nanocages ($3.81 \pm 1.08$)[12a] and the GS-AuNPs at the same time point (Figure 2c), thus suggesting that PEGylation can enhance the EPR effect relative to zwitterionization. Although the EPR effect is often considered to be a unique strength of NPs that are not renal-clearable because these can escape rapid kidney filtration and remain in the blood at a high concentration,[1f,15] the observed high tumor/blood ratio of the PEG-AuNPs clearly indicates that a strong EPR effect can also be achieved by tuning the surface chemistry of renal-clearable NPs.

The enhanced EPR effect of the PEG-AuNPs is fundamentally due to prolonged retention time and a high concentration of the AuNPs in the blood. Classical two-compartment pharmacokinetics were observed for the PEG-AuNPs, with distribution half-life ($t_{1/2\alpha}$) and elimination half-life ($t_{1/2\beta}$) values of ($56.1 \pm 9.7$) min and ($9.2 \pm 3.9$) h, respectively (Figure 2d). The $t_{1/2\alpha}$ of the PEG-AuNPs was an order of magnitude longer than that of the GS-AuNPs ($5.4 \pm 1.2$ min) even though the $t_{1/2\beta}$ values for the PEG-AuNPs and GS-AuNPs ($8.5 \pm 2.1$ h) were comparable. In addition, the area under the curve (AUC) for the PEG-AuNPs (142.8 %ID h g$^{-1}$) was three times larger than that for the GS-AuNPs (47.2 %ID h g$^{-1}$) at 24 h p.i. The large AUC of the PEG-AuNPs in the blood is fundamentally responsible for their high tumor-targeting efficiency.

Subsequently, the kinetics of passive tumor-targeting by the NIR-emitting PEG-AuNPs were measured through the real-time imaging of particle accumulation in the MCF-7 tumors. While the tumor area was hardly distinguishable directly after iv injection of the particles, it became visible over time (Figure 3a). After iv injection of the PEG-AuNPs, it took over 12 h for the tumor area to reach the contrast index (CI) threshold (CI = 2.5; Figure 3b),[16] a general parameter for the evaluation of imaging quality.[17] This was much longer than the time needed for the GS-AuNPs (ca. 3 h).[11h] To gain a more quantitative understanding of the tumor targeting of the PEG-AuNPs, we quantified and compared the accumulation and clearance kinetics of the PEG-AuNPs with those of the GS-AuNPs. The fluorescence intensities of normal tissues reached a maximum at 5 h p.i. with the PEG-AuNPs (Figure 3c), whereas it took less than 10 min for the GS-AuNPs to reach their maximum.[11h] The clearance kinetics of the PEG-AuNPs in normal tissues exhibited a monoexponential decay with a half-life of ($4.1 \pm 0.2$) h (Figure 3c), more than five

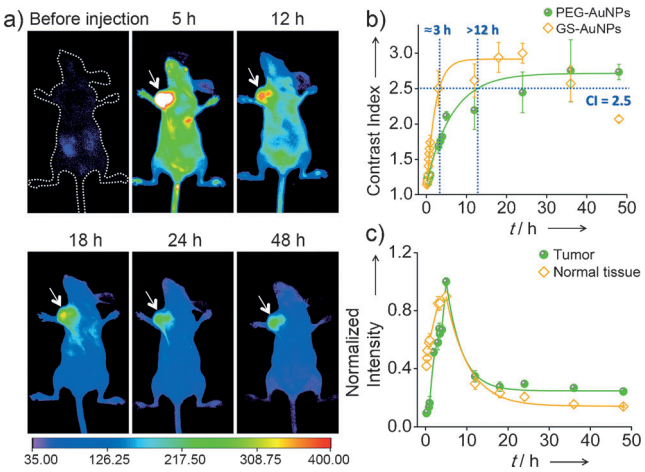


***Figure 3.*** Kinetics for the passive tumor targeting of the PEG-AuNPs in nude mice bearing MCF-7 tumors. a) In vivo NIR fluorescence images of the mouse iv injected with PEG-AuNPs at 5, 12, 18, 24, and 48 h p.i. (the arrow shows the tumor location). b) Time-dependent CI of the tumor area after iv injection of the PEG-AuNPs or GS-AuNPs. c) Accumulation and retention kinetics of the PEG-AuNPs in tumor and normal tissues.

times longer than that of the GS-AuNPs ($(43.4 \pm 6.6)$ min)[11h]. Subsequent analysis of the tumor retention kinetics showed that the PEG-AuNPs reached their maximum accumulation at the tumor site at 5 h p.i., thus taking more than seven times longer than the GS-AuNPs (ca. 40 min),[11h] a result consistent with their slow diffusion in the normal tissues. Once the emission intensity of the tumor reached its maximum, the PEG-AuNPs, like many other NPs[13a] or nanosized proteins,[1e] were slowly released back into the blood stream. The tumor clearance kinetics of the PEG-AuNPs can be fitted to a monoexponential decay with a half-life of ($3.7 \pm 0.8$) h. Interestingly, unlike the GS-AuNPs, of which more than 76 % remained in the tumor at 24 h p.i., only about 30 % of the PEG-AuNPs were retained in the tumor after the same period of time.

The slow clearance of the PEG-AuNPs from the normal tissues was also consistent with their renal clearance kinetics. While the GS-AuNPs were rapidly excreted into the bladder, and the fluorescence intensity of the bladder area reached its

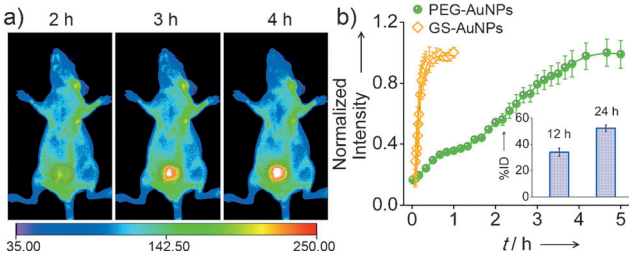


***Figure 4.*** Renal clearance kinetics of the PEG-AuNPs in nude mice. a) In vivo NIR fluorescence images of the nude mouse iv injected with the PEG-AuNPs collected at 2, 3, and 4 h p.i. (the circle indicates the bladder area). b) Renal clearance kinetics of the PEG-AuNPs and GS-AuNPs (inset: PEG-AuNPs found in the urine measured by ICP-MS at 12 and 24 h p.i.).

maximum within 1 h p.i., very little accumulation of the PEG-AuNPs in the bladder was observed in the same time window. The bladder area started to become visible at 3 h p.i., and reached maximum intensity at 5 h p.i. (Figure 4). The urine collected within the first 5 h p.i. from the mouse intravenously injected with the PEG-AuNPs showed a strong NIR emission with the same wavelength as the PEG-AuNPs before injection, thus further confirming that the particles were renal-clearable and fairly stable during circulation in the body (Figures S7 and S8 in the Supporting Information). Although the PEG-AuNPs showed slow renal clearance in the initial stage, a comparable amount of PEG-AuNPs and GS-AuNPs[11g] were found in the urine 24 h p.i., thus suggesting that the slow clearance of the PEG-AuNPs from normal tissues results from their slow diffusion in the body rather than delayed RES uptake.

In summary, we synthesized the first renal-clearable NIR-emitting PEGylated AuNPs through a facile one-step method, and these NPs exhibit photophysical properties and core size almost identical to zwitterionic GS-AuNPs. Systematic studies of the renal clearance, pharmacokinetics, and passive tumor targeting of PEG-AuNPs and GS-AuNPs in mice bearing MCF-7 tumors showed that the PEG-AuNPs can effectively target tumors with an efficiency three times higher than that of the GS-AuNPs, although the two of them exhibited comparable low RES uptake. These results were further confirmed in prostate PC-3 tumor xenografts (Figure S9 in the Supporting Information), thus suggesting that the observed differences in tumor targeting between PEGylation and zwitterionization are a general phenomenon in renal-clearable luminescent AuNPs and can be generalized to other tumor models. The high tumor-targeting efficiency of the PEG-AuNPs is fundamentally a result of the fact that PEGylation can enhance the EPR effect of renal-clearable luminescent AuNPs relative to zwitterionization by increasing their retention time and concentration in the blood (large AUC). However, the limitation of PEGylation in tumor imaging is that it took much longer for the PEG-AuNPs to reach the desired CI threshold than it took the zwitterionic GS-AuNPs because of the slow tumor accumulation and normal-tissue clearance of the PEG-AuNPs. These differences in the tumor targeting of luminescent AuNPs imply that PEGylated AuNPs are potentially more suitable for cancer therapy owing to their high targeting efficiency and long tumor retention, whereas zwitterionic GS-AuNPs have potential for use in cancer diagnosis owing to their short detection time and rapid clearance from normal tissues.

Although we successfully unraveled the different effects of zwitterionization and PEGylation on the tumor targeting and renal clearance of NIR-emitting AuNPs, fundamental understanding of the origin of these differences still demands further study. In addition, a recent interesting observation of renal clearance of silica NPs with a size of over 50 nm,[18] which is much larger than the kidney filtration threshold (ca. 5.5 nm), points to the importance of a more thorough understanding of the renal clearance of NPs. Nevertheless, the observed differences in tumor targeting and renal clearance between these two distinct surface modifications are expected to help in the development of a new generation of renal-clearable inorganic NPs with minimized nanotoxicity, so that they can eventually be translated into clinical practice.

Received: May 23, 2013
Revised: July 31, 2013
Published online: October 9, 2013

**Keywords:** nanoparticles · PEGylation · renal clearance · surface chemistry · tumor targeting

[1] a) Y. Wang, Y. Liu, H. Luehmann, X. Xia, P. Brown, C. Jarreau, M. Welch, Y. Xia, *ACS Nano* **2012**, *6*, 5880 – 5888; b) J. Y. Chen, C. Glaus, R. Laforest, Q. Zhang, M. X. Yang, M. Gidding, M. J. Welch, Y. N. Xia, *Small* **2010**, *6*, 811 – 817; c) J. V. Jokerst, T. Lobovkina, R. N. Zare, S. S. Gambhir, *Nanomedicine* **2011**, *6*, 715 – 728; d) J. Della Rocca, R. C. Huxford, E. Comstock-Duggan, W. B. Lin, *Angew. Chem.* **2011**, *123*, 10514 – 10518; *Angew. Chem. Int. Ed.* **2011**, *50*, 10330 – 10334; e) Y. Matsumura, H. Maeda, *Cancer Res.* **1986**, *46*, 6387 – 6392; f) A. K. Iyer, G. Khaled, J. Fang, H. Maeda, *Drug Discovery Today* **2006**, *11*, 812 – 818; g) H. Hong, Y. Zhang, J. Sun, W. Cai, *Nano Today* **2009**, *4*, 399 – 413.

[2] a) S. Kommareddy, M. Amiji, *J. Pharm. Sci.* **2007**, *96*, 397 – 407; b) F. Alexis, E. Pridgen, L. K. Molnar, O. C. Farokhzad, *Mol. Pharm.* **2008**, *5*, 505 – 515.

[3] M. L. Schipper, G. Iyer, A. L. Koh, Z. Cheng, Y. Ebenstein, A. Aharoni, S. Keren, L. A. Bentolila, J. Q. Li, J. H. Rao, X. Y. Chen, U. Banin, A. M. Wu, R. Sinclair, S. Weiss, S. S. Gambhir, *Small* **2009**, *5*, 126 – 134.

[4] a) K. L. Aillon, Y. Xie, N. El-Gendy, C. J. Berkland, M. L. Forrest, *Adv. Drug Delivery Rev.* **2009**, *61*, 457 – 466; b) M. A. Dobrovolskaia, S. E. McNeil, *Nat. Nanotechnol.* **2007**, *2*, 469 – 478; c) H. Kareem, K. Sandstrom, R. Elia, L. Gedda, M. Anniko, H. Lundqvist, M. Nestor, *Tumour Biol.* **2010**, *31*, 79 – 87.

[5] R. R. Arvizo, O. R. Miranda, D. F. Moyano, C. A. Walden, K. Giri, R. Bhattacharya, J. D. Robertson, V. M. Rotello, J. M. Reid, P. Mukherjee, *PLoS One* **2011**, *6*, e24374.

[6] a) G. J. Kelloff, J. M. Hoffman, B. Johnson, H. I. Scher, B. A. Siegel, E. Y. Cheng, B. D. Cheson, J. O'Shaughnessy, K. Z. Guyton, D. A. Mankoff, L. Shankar, S. M. Larson, C. C. Sigman, R. L. Schilsky, D. C. Sullivan, *Clin. Cancer Res.* **2005**, *11*, 2785 – 2808; b) C. Colosimo, P. Demaerel, P. Tortori-Donati, C. Christophe, M. Van Buchem, B. Hogstrom, G. Pirovano, N. Shen, M. A. Kirchin, A. Spinazzi, *Pediatr. Radiol.* **2005**, *35*, 501 – 510.

[7] M. Longmire, P. L. Choyke, H. Kobayashi, *Nanomedicine* **2008**, *3*, 703 – 717.

[8] H. S. Choi, B. I. Ipe, P. Misra, J. H. Lee, M. G. Bawendi, J. V. Frangioni, *Nano Lett.* **2009**, *9*, 2354 – 2359.

[9] A. A. Burns, J. Vider, H. Ow, E. Herz, O. Penate-Medina, M. Baumgart, S. M. Larson, U. Wiesner, M. Bradbury, *Nano Lett.* **2009**, *9*, 442 – 448.

[10] M. Benezra, O. Penate-Medina, P. B. Zanzonico, D. Schaer, H. Ow, A. Burns, E. DeStanchina, V. Longo, E. Herz, S. Iyer, J. Wolchok, S. M. Larson, U. Wiesner, M. S. Bradbury, *J. Clin. Invest.* **2011**, *121*, 2768 – 2780.

[11] a) H. S. Choi, W. Liu, P. Misra, E. Tanaka, J. P. Zimmer, B. I. Ipe, M. G. Bawendi, J. V. Frangioni, *Nat. Biotechnol.* **2007**, *25*, 1165 – 1170; b) H. S. Choi, W. H. Liu, F. B. Liu, K. Nasr, P. Misra, M. G. Bawendi, J. V. Frangioni, *Nat. Nanotechnol.* **2010**, *5*, 42 – 47; c) C. Zhou, C. Sun, M. X. Yu, Y. P. Qin, J. G. Wang, M. Kim, J. Zheng, *J. Phys. Chem. C* **2010**, *114*, 7727 – 7732; d) M. X. Yu, C. Zhou, J. B. Liu, J. D. Hankins, J. Zheng, *J. Am. Chem. Soc.* **2011**, *133*, 11014 – 11017; e) J. Zheng, C. Zhou, M. Yu, J. Liu, *Nanoscale* **2012**, *4*, 4073 – 4083; f) C. Zhou, M. Long, Y. Qin, X. Sun, J.

  

Zheng, *Angew. Chem.* **2011**, *123*, 3226 – 3230; *Angew. Chem. Int. Ed.* **2011**, *50*, 3168 – 3172; g) C. Zhou, G. Y. Hao, P. Thomas, J. B. Liu, M. X. Yu, S. S. Sun, O. K. Oz, X. K. Sun, J. Zheng, *Angew. Chem.* **2012**, *124*, 10265 – 10269; *Angew. Chem. Int. Ed.* **2012**, *51*, 10118 – 10122; h) J. B. Liu, M. X. Yu, C. Zhou, S. Y. Yang, X. H. Ning, J. Zheng, *J. Am. Chem. Soc.* **2013**, *135*, 4978 – 4981.

[12] a) Y. Wang, Y. Liu, H. Luehmann, X. Xia, D. Wan, C. Cutler, Y. Xia, *Nano Lett.* **2013**, *13*, 581 – 585; b) G. Zhang, Z. Yang, W. Lu, R. Zhang, Q. Huang, M. Tian, L. Li, D. Liang, C. Li, *Biomaterials* **2009**, *30*, 1928 – 1936; c) G. S. Hong, J. T. Robinson, Y. J. Zhang, S. Diao, A. L. Antaris, Q. B. Wang, H. J. Dai, *Angew. Chem.* **2012**, *124*, 9956 – 9959; *Angew. Chem. Int. Ed.* **2012**, *51*, 9818 – 9821.

[13] a) S. D. Perrault, C. Walkey, T. Jennings, H. C. Fischer, W. C. W. Chan, *Nano Lett.* **2009**, *9*, 1909 – 1915; b) P. Puvanakrishnan, J. Park, D. Chatterjee, S. Krishnan, J. W. Tunnell, *Int. J. Nanomed.* **2012**, *7*, 1251 – 1258.

[14] M. Wang, M. Thanou, *Pharmacol. Res.* **2010**, *62*, 90 – 99.

[15] a) S. Modi, J. Prakash Jain, A. J. Domb, N. Kumar, *Curr. Pharm. Des.* **2006**, *12*, 4785 – 4796; b) H. Maeda, *Adv. Enzyme Regul.* **2001**, *41*, 189 – 207.

[16] a) O. A. Andreev, A. D. Dupuy, M. Segala, S. Sandugu, D. A. Serra, C. O. Chichester, D. M. Engelman, Y. K. Reshetnyak, *Proc. Natl. Acad. Sci. USA* **2007**, *104*, 7893 – 7898; b) E. L. Zhang, C. Zhang, Y. P. Su, T. M. Cheng, C. M. Shi, *Drug Discovery Today* **2011**, *16*, 140 – 146.

[17] T. Jiang, E. S. Olson, Q. T. Nguyen, M. Roy, P. A. Jennings, R. Y. Tsien, *Proc. Natl. Acad. Sci. USA* **2004**, *101*, 17867 – 17872.

[18] a) C. Fu, T. Liu, L. Li, H. Liu, D. Chen, F. Tang, *Biomaterials* **2013**, *34*, 2565 – 2575; b) X. He, H. Nie, K. Wang, W. Tan, X. Wu, P. Zhang, *Anal. Chem.* **2008**, *80*, 9597 – 9603; c) M. Gary-Bobo, Y. Mir, C. Rouxel, D. Brevet, I. Basile, M. Maynadier, O. Vaillant, O. Mongin, M. Blanchard-Desce, A. Morere, M. Garcia, J. O. Durand, L. Raehm, *Angew. Chem.* **2011**, *123*, 11627 – 11631; *Angew. Chem. Int. Ed.* **2011**, *50*, 11425 – 11429.